JOURNAL OF MATERIALS SCIENCE 19 (1984) 3375–3388

Electron-microscopical observation of crystal growth in amorphous $Fe_{75}B_{25}$ alloy

YOSHIAKI KATAO*, MICHIO KIRITANI†, FRANCISCO EIICHI FUJITA
Department of Material Physics, Faculty of Engineering Science, Osaka University, Toyonaka, Osaka 560, Japan

Amorphous ribbons of $Fe_{75}B_{25}$ alloy were made by melt-spinning and their crystallization process was observed *in situ* under a transmission electron microscope (TEM). Especially, the growth rate of bct Fe_3B crystals was measured with high precision at various temperatures, and the kinetics of the movement of the amorphous–crystalline interface was examined. Differing from the amorphous $Fe_{86}B_{14}$ alloy studied earlier and other Fe–B alloys with compositions not close to the 3:1 stoichiometry, crystal growth in the $Fe_{75}B_{25}$ alloy showed a perfect linearity against time, with no relaxation phenomena being observed. The linear growth was not disturbed by the small concentration deviations or the crystal orientations. When the annealing temperature was changed stepwise up and down between 190° C to 380° C, the linear growth was maintained at each temperature and no temperature hysteresis of the growth rate appeared. The Arrhenius plots of the growth rates gave an apparent activation energy of about 2 eV, but the plotted lines were not exactly straight but upward concave and/or convex. Theoretical analysis of the reaction kinetics of the amorphous–crystalline boundary movement was based on either the concept of multiple processes connected in series or in parallel or of the temperature-dependent activation energy of the process. Good agreement between the calculated and experimental curves was obtained and underlying mechanisms of the growth process were considered and discussed. It was concluded that the crystal growth process of amorphous $Fe_{75}B_{25}$ alloy is not controlled by long-range diffusion but presumably by small concentration deviations and local fluctuations of concentration and structural order.

1. Introduction

Crystallization behaviour of amorphous alloys has been extensively studied, mainly by measuring the bulk properties such as the electrical resistivity [1, 2], heat evolution [3], length change [4–6] and magnetization [7]. However, the reactions at the interface between the crystalline and amorphous phases, which sometimes play the main role in the crystallization process, are not always apparent from bulk property measurements. The X-ray diffraction method [8] is useful for structural analysis and measurement of the bulk rate of crystallization, and the measurement of the diffusion rate in the amorphous structure before crystallization using radiation techniques [9–11] is also useful for understanding the crystallization behaviour. However, these two are still not always sufficient to give an insight into the mechanism of crystallization. Other useful techniques are, for instance, Mössbauer spectroscopy [12–15] and EXAFS [16], which enable us to study the structural changes associated with crystallization but not the kinetic reactions at the amorphous–crystalline boundaries. In this respect, *in situ* electron microscopical observation gives more localized and direct examination of the reactions, since it can measure the growth rate of every crystalline particle in the amorphous phase at

*Present address: Central Technical Research Laboratory, Sumitomo Steel Co., Amagasaki 660, Japan.
†Present address: Department of Precision Mechanics, Hokkaido University, Sapporo 060, Japan.

0022–2461/84 $03.00 + .12

every moment. Herold and Köster [17] first measured the rate of crystallization in some amorphous alloys by electron microscopy, and found an apparent activation energy of about 2 eV, the alloy concentration dependence of the growth rate, and the diffusion coefficient of metalloid atoms in the amorphous phase.

The authors have reported in a previous paper [18] that the growth rate of the body-centred tetragonal (bct) Fe_3B crystals in amorphous Fe–14 at% B alloy gradually changed with the elapsed annealing time due to the change in composition of the amorphous matrix produced by the unavoidable long-range diffusion of boron atoms. Therefore, although the apparent activation energy was found to be about 2 eV in agreement with the result of Herold and Köster [17], the compositional change of the amorphous matrix surrounding the growing Fe_3B crystals made the process complicated and further analysis of the reactions at the amorphous–crystalline interface was not achieved.

In the present study, the nucleation and growth of Fe_3B crystals in the amorphous Fe–25 at% B alloy corresponding to 3:1 stoichiometry were measured by an *in situ* annealing technique in TEM observation, and the kinetics and mechanism of rearrangement of atoms at the amorphous–crystalline interface could be discussed in more detail than in the previous study.

2. Experimental procedure

Iron–boron alloys with the desired concentrations around the stoichiometric composition, $Fe_{75}B_{25}$, were prepared by melting the weighed amounts of electrolytic iron and pure boron over a water-cooled copper hearth in an argon atmosphere in an arc-melting furnace. Repeated melting and turning over were useful for homogenizing. The melt buttons were about 30 g in weight and deviations from the intended compositions checked by measuring the weight loss after the melting were less than 0.1 at%. The weighing method was sometimes better than the chemical analysis. Remelting of the crushed mother alloys before spinning was done in a quartz tube with a nozzle in an argon atmosphere, and ribbons of amorphous Fe–B alloys containing 24.0, 24.3, 24.7, 25.0 and 25.5 at% B were made by melt spinning onto a copper wheel of 200 mm diameter rotating at a speed of 4500 r.p.m. The prepared ribbons were about 1 mm wide and 15 μm thick, and the surface had no trace of contamination. The ribbons were cut into pieces 10 mm long. The surface undulations were removed by mechanical polishing and then they were electrolytically thinned to obtain the wedge-shaped regions suitable for electron microscopical observation. The thinned specimens were annealed on a heating stage in a transmission electron microscope, JEM-200CX, operated at 200 kV, and the *in situ* observation of crystallization from the amorphous phase was performed. Special attention was paid to avoid an extraneous local temperature rise caused by the electron beam. For this purpose, the electron beam was sufficiently diverged so as to avoid heating the observation area by more than 30 degrees and not to produce any significant temperature gradient in it.

The heat treatment and observation of the specimens in the electron microscope were performed as follows. The specimen on a heating stage with a universal goniometer was quickly heated at a rate of a few degrees per second up to about ten degrees below the crystallization temperature. Then, the heating rate was lowered to a few degrees per minute until the crystallization temperature was reached and crystallites of Fe_3B with the Ni_3P-type bct structure, suitable for observation, appeared. As soon as a desirable crystallite was found, the temperature was reset and kept at a level suitable for isothermal annealing. The temperature was manually controlled and its accuracy was within ± 0.5 degrees. In order to find the temperature dependence and the temperature hysteresis of the growing rate of the crystallite, the annealing temperature of the specimen was raised and reduced successively and alternately, as will be described later. The total range of the annealing temperatures was from 190 to 380° C, and the annealing time at each temperature was from about 1 min to 4 h. The temperature range for the observation of one crystallite was as wide as 120 degrees. Sometimes, the annealing temperature was changed stepwise to find the activation energy of the growth process, as will be shown later. The shapes of the crystallites were not always circular but sometimes oval or polyhedral, reflecting the crystal anisotropy. To determine the growth rate of a crystallite, a series of photographs were taken during an isothermal anneal and the length change of the longest axis of the crystallite was measured on the enlarged photographs by using a ruler with an accuracy of

± 0.1 mm, which corresponds to about ± 10 nm in real length. Determination of crystal structures and examination of the degree of perfection of the crystallites were performed using the selected-area electron diffraction technique. The amorphous structure was checked also by electron diffraction and microscopy.

The electron microscopical observation has the advantage that both the overall and local changes can be examined and the growth rate of the amorphous–crystalline interface can be measured over a wide range from 10^{-4} to $10\,\mu m\,min^{-1}$, which is not obtainable by other techniques, but, on the other hand, the surface effect or the thickness effect on the crystallization behaviour must be taken into consideration. For that purpose, bulk specimens of the same origin were prepared, heat treated, thinned, and subjected to X-ray and electron microscope measurements to see the difference from the specimens thinned *ab initio*.

3. Experimental result

3.1. Morphology of the observed crystallites

Upon heating the above-mentioned amorphous Fe–B alloy specimens to above 300° C, crystallization took place in the following different forms with different probabilities depending on marginal differences in experimental conditions.

1. At about 320° C, eutectoid agglomeration of tetragonal Fe_2B and α-iron crystallites with irregular asterisk shapes, which corresponds to the final form of phase decomposition of this material, appeared as shown in Fig. 1. Crystallization in this form was frequently observed with the specimens containing 25.5 at % B, which have boron in excess of the 3:1 stoichiometry of Fe_3B.

2. The specimens deficient in boron, i.e. 24.0, 24.3, and 24.7 at % B, mostly produced bct Fe_3B crystallites with clear and smooth boundaries. The growth rate measurement was carried out only on crystallites of this type. They always appeared as single crystals, as the continuous bend contours in Figs. 2 and 5 show, and their shapes were circular, oval, or polyhedral with round corners, depending on the crystal orientations in the specimen film, as the diffraction patterns accompanying Fig. 2 show. The polyhedra were always elongated in the ⟨1 1 0⟩ directions, corresponding to the axes of easy growth, and the measurement of the growth rate was done mainly along the longest direction. The growth along the ⟨1 0 0⟩ directions as the secondary preferential axes was also often observed. The lattice parameters of the tetragonal Fe_3B crystallites appeared as dendritic clusters or were $a = 0.864$ nm and $c = 0.430$ nm, which did not change between specimens with different compositions and different annealing times. Subgrains forming small-angle boundaries were commonly observed in all the crystallites, but their influence on crystal growth was not found at all.

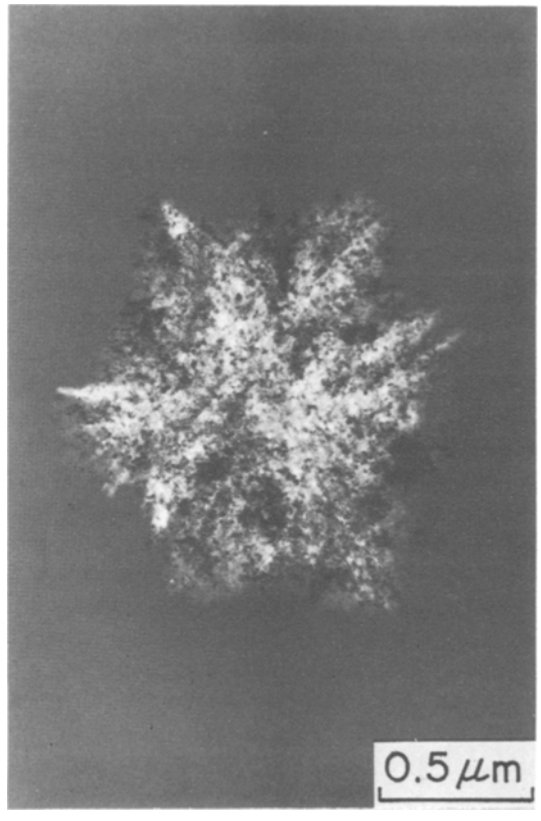

Figure 1 Eutectoid agglomeration of bct Fe_2B and α-iron crystallites as a crystallization form from amorphous Fe–25.5 at % B alloy at 320° C.

3. Very small α-iron particles of the order of 10 nm in diameter, which had appeared prior to the Fe_3B crystallization in the previous experiment on the amorphous Fe–14 at % B alloy [18], did not appear independently of Fe_3B crystallites but only in their interior at their crystallization temperature, about 320° C. The emergence of α-iron particles was most probably necessitated to compensate the deviation from the 3:1 stoichiometric composition. For instance, when iron particles of 10 nm in diameter are dispersed at a mean separation of say 80 nm, the amount of precipitate of iron will be about 0.1%, which is of the same order

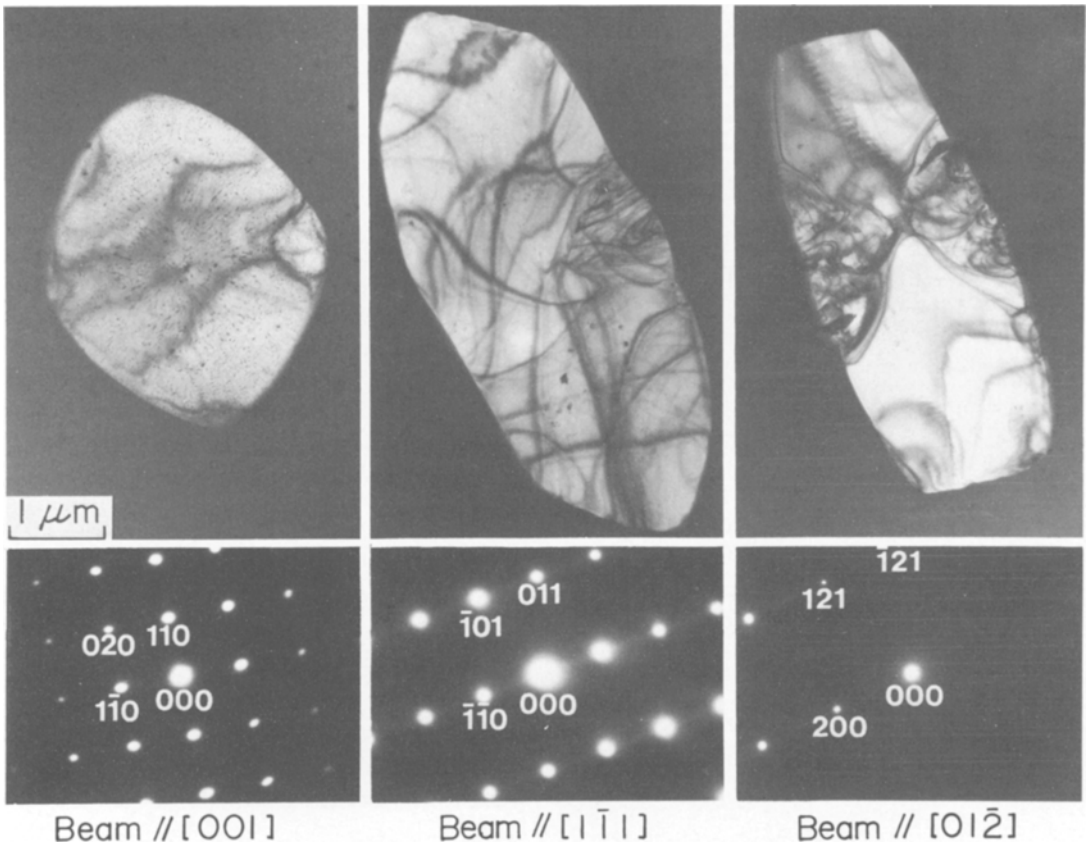

Figure 2 The bct Fe_3B crystallites with different crystal orientations in amorphous 25 at % B alloy film.

as the excess amount of iron in the specimens under consideration. No lattice parameter change during the crystallization process was observed, nor were they found to have any clear arresting effect on the growth process of the Fe_3B crystals. They are seen as small dark spots in Figs. 2, 3a and 5, and more clearly as bright spots with different shapes in the dark-field image of the interior of a Fe_3B crystal in Fig. 3b.

4. In Fe–25.0 at % B specimens, orthorhombic

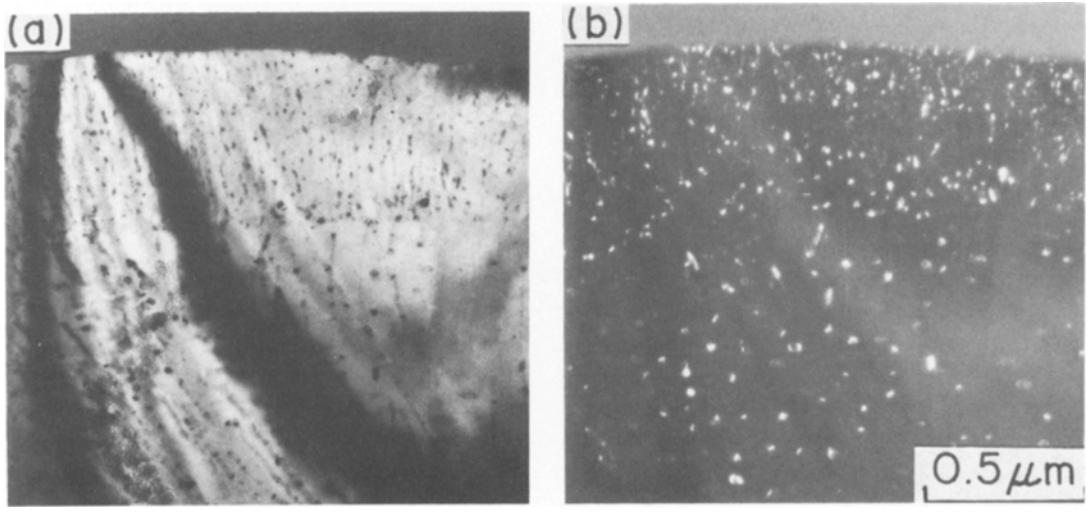

Figure 3 (a) A bright and (b) dark field electron image of a Fe_3B crystal containing α-iron particles. Note that α-iron particles do not appear in the amorphous matrix.

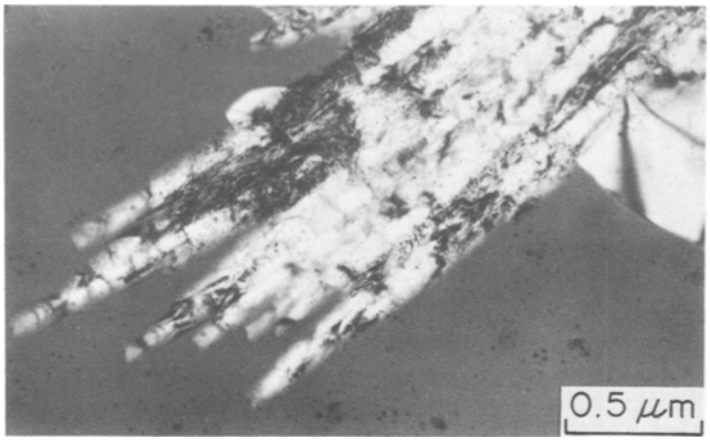

Figure 4 Orthorhombic Fe_3B crystallites growing in parallel in amorphous Fe–25.0 at % B alloy.

Fe_3B crystallites appeared as dendritic clusters or parallel-grown bundles, as shown in Fig. 4, especially when the annealing temperature was comparatively low and the annealing time long.

The above variety in morphology of crystallization was almost unavoidable; sometimes, different forms appeared together and the forms changed from place to place, presumably as a result of concentration fluctuations. However, comparison with crystallites of other types, bct Fe_3B crystallites appeared most frequently with the simplest shapes, making it easy to measure the movement of the phase boundary. Since the boundaries penetrated vertically from the top to the bottom surface of the thin film specimens, the accuracy in determining the boundary position reached ± 10 nm or less in the electron microscopical observation. The growth of crystallites observed in this way was essentially two-dimensional, and the measured growth rate of the crystallites was in one dimension as far as crystallites larger than 0.5 μm or so in diameter were measured.

The process of nucleation of crystallites from the amorphous phase is an essential and interesting problem as well as that of crystal growth. For that purpose, however, a more dynamic and higher resolution observation [19], such as by movie camera with greatest magnification on a very thin specimen, and a theoretical analysis of the image formation [20], will be required. Hence, the present investigation is concerned only with the observation of growth of crystallites and its kinetic analysis.

3.2. Growth rate of bcc Fe_3B crystallites

In Fig. 5 is shown a typical *in situ* observation of the growth of a bct Fe_3B crystallite in the Fe–25 at % B amorphous specimen at 312° C. As distinct from the previous observation on the Fe–14 at % B specimen [18], the growth was perfectly linear, as plotted in Fig. 6, exhibiting a constant isothermal growth rate from start to finish of the observation, i.e. from less than 1 μm to more than 10 μm in diameter, independent of the foil thickness, which varied from zero to ~ 500 nm in the wedge-shaped specimen prepared for electron microscopy. The linear growth was not influenced by the small concentration deviations and conserved along any axis of the growing polyhedral crystallites. In addition, when two crystallites happened to appear together in a short distance, they grew linearly without interference until they met each other to make a crystal–crystal boundary. The above observations strongly suggested that the growth of the crystallite or the motion of the phase boundary was driven not by the long range atomic transport but by the short range atomic movements or rearrangements very near or at the boundary.

In order to obtain the temperature dependence of the growth rate, the temperature of the heating stage in the electron microscope was changed stepwise and observations were made at each temperature, as shown in Fig. 7. The growth rates at various temperatures thus obtained are plotted on a logarithmic scale against reciprocal temperature, as shown in Fig. 8. Note that the temperature was not a monotonic rising or falling but an alternate up and down, as indicated by the temperatures entered in Fig. 7 and the numerals denoting the order of observation in Fig. 8. By performing an alternate back-and-forth isothermal observations on all the specimens, it was confirmed that no temperature hysteresis existed in the growth rate

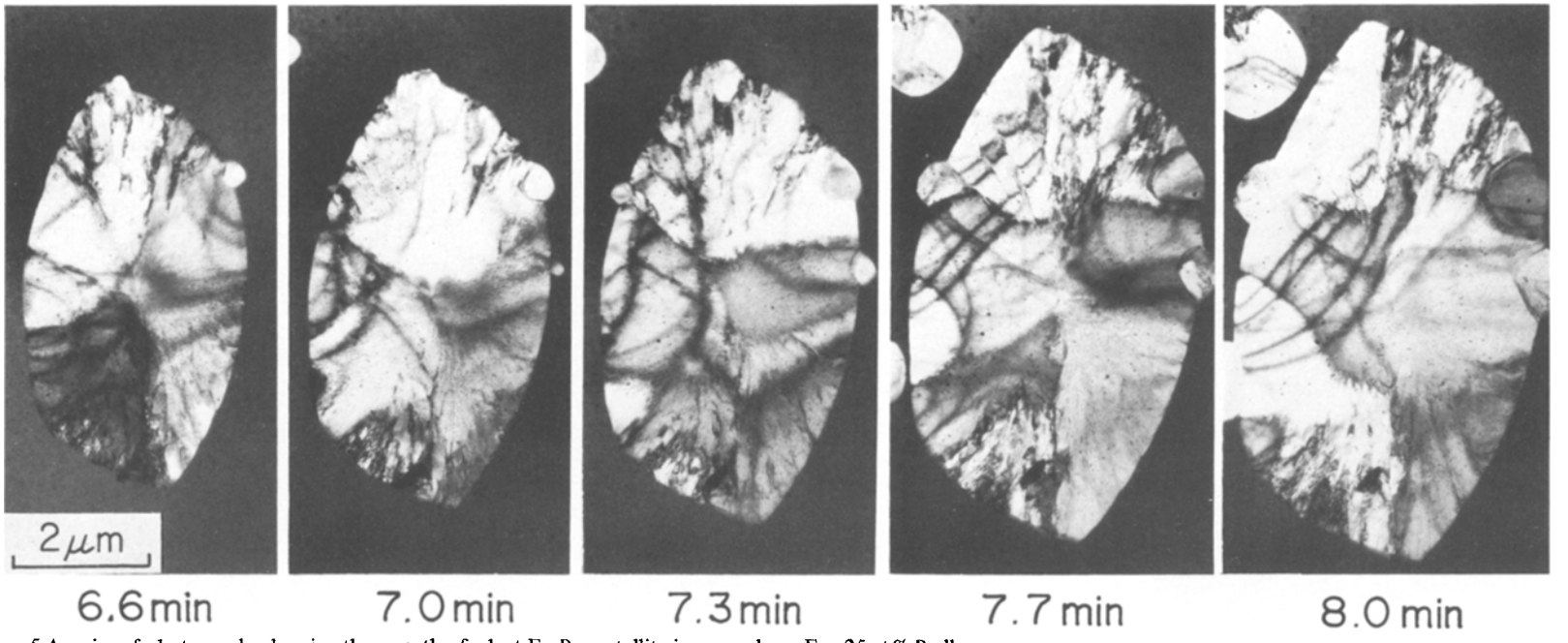

Figure 5 A series of photographs showing the growth of a bct Fe_3B crystallite in amorphous Fe–25 at % B alloy.

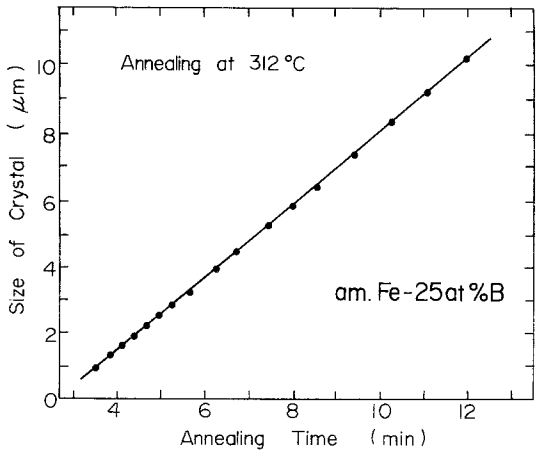

Figure 6 Growth curve of a bct Fe_3B crystallite in amorphous Fe–25 at % B alloy at 312° C.

and, therefore, the rate was determined uniquely at each temperature. The activation energy of the process determined from the inclination of the Arrhenius plot in Fig. 8 was about 2.0 eV, which was the same as in the 14 at % B alloy. By extending the experiment, however, to wider temperature ranges and different specimens, some more complicated situations appeared. For instance, a considerable part of the growth rate observations, summarized in Fig. 9, show that the rates differ from specimen to specimen by one or two orders of magnitude almost independently of the alloy compositions. The Arrhenius plots are not always straight lines but sometimes show upward and sometimes downward curvature. The apparent activation energies are accordingly different even along one growth rate line; for instance, growth of a specimen of 25.0 at % B denoted by (b) shows the activation energy of 1.7 eV at around 320° C, 2.0 eV at 280° C, and 2.26 eV at 240° C, as written in the figure. It must be further noted that three specimens with the same alloy composition, 25.0 at % B, behaved differently; specimen (a) showed an upward concave growth rate curve and an extremely low activation energy of 1.0 eV at low temperatures, the above-mentioned specimen (b) showed an upward convex curve with the highest activation energy of 2.3 eV at the lowest temperatures, and specimen (c) a nearly straight line with 1.7 eV. Inflection of curves also appeared as on the specimens of 24.0 and 24.4 at % B in the figure. These differences in the growth behaviour observed in specimens which were more or less identical in composition and production conditions, are quite suggestive and will be taken into consideration when the elementary processes in the crystal growth from the amorphous phase are discussed in the following section.

4. Discussion

4.1. Effect of boron excess or deficit on the growth of Fe_3B crystallites

Herold and Köster [17] previously reported that the growth speeds of bct Fe_3C crystallites in the amorphous Fe–20 at % B, Fe–25 at % B, and Fe–26 at % B alloys were in the ratio of 1/3: 1: 1/5. Since the nucleation and growth of a compound crystal must be the easiest when the stoichiometric condition is maintained in both the amorphous matrix and newly born crystals, the highest growth speed in the 25 at % B alloy is quite understandable. It has been reported by Shingu *et al.* [21] that the first precipitating α-iron particles from the amorphous Fe–12 at % B alloy were supersaturated with boron and they continuously

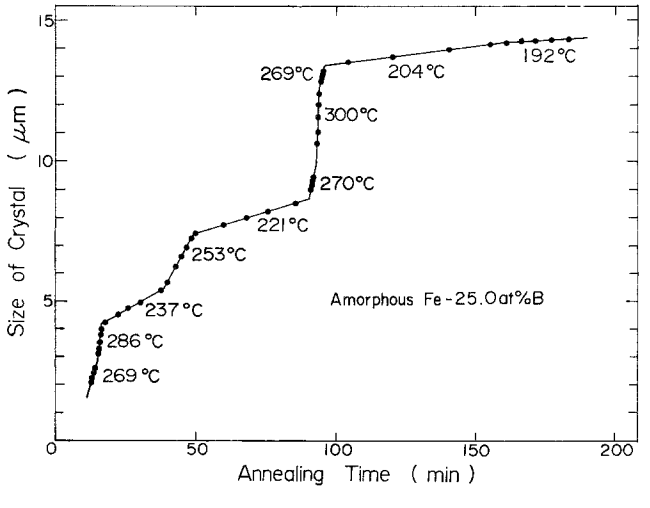

Figure 7 Growth of a bct Fe_3B crystallite in an amorphous Fe–25.0 at % B specimen at various temperatures. Note that the temperature is changed in irregular order.

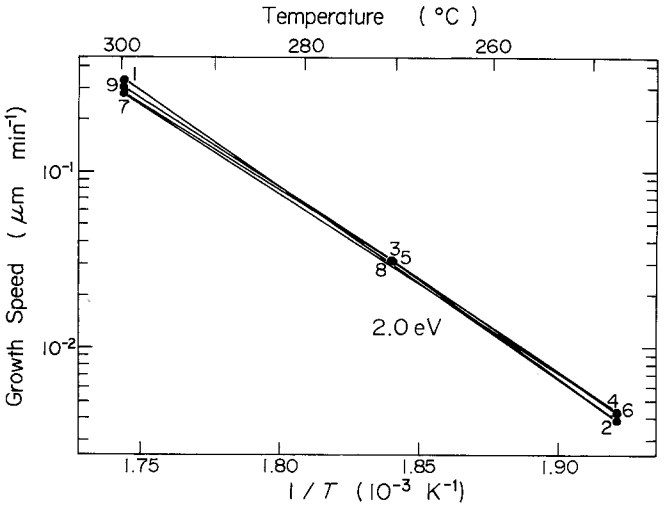

Figure 8 An example of Arrhenius plot of the growth rates at various temperatures. Numerals in the figure show the order of observations. The inclination of the lines give the activation energy of about 2.0 eV.

discharged the boron during subsequent anneals. The boron intake into α-iron particles and its later release and consequently accumulation in the amorphous matrix has also been observed by Ruckman *et al.* [22] In accordance with the above experimental results, it was observed in the previous study on the Fe–14 at% B amorphous alloy [18] that the growth rate of bct Fe_3B crystallittes was sometime accelerated and sometimes retarded during the time of precipitation, most probably being influenced by the change of boron concentration in the amorphous matrix. Actually, from the temperature dependence of the relaxation time of the growth-rate deceleration, an activation energy of 4.8 eV, which differed from that of the growth rate itself, 2.0 eV, was obtained, and, by assuming a diffusion process controlling the growth rate change, the diffusivity of boron in the amorphous phase was estimated, giving good agreement with the direct measurement value of Cahn *et al.* [23].

The present study on the Fe–B amorphous alloys with almost 25 at% boron concentrations found a completely different behaviour in the growth process of Fe_3B crystals. For instance, as mentioned before and shown in Fig. 6, the iso-

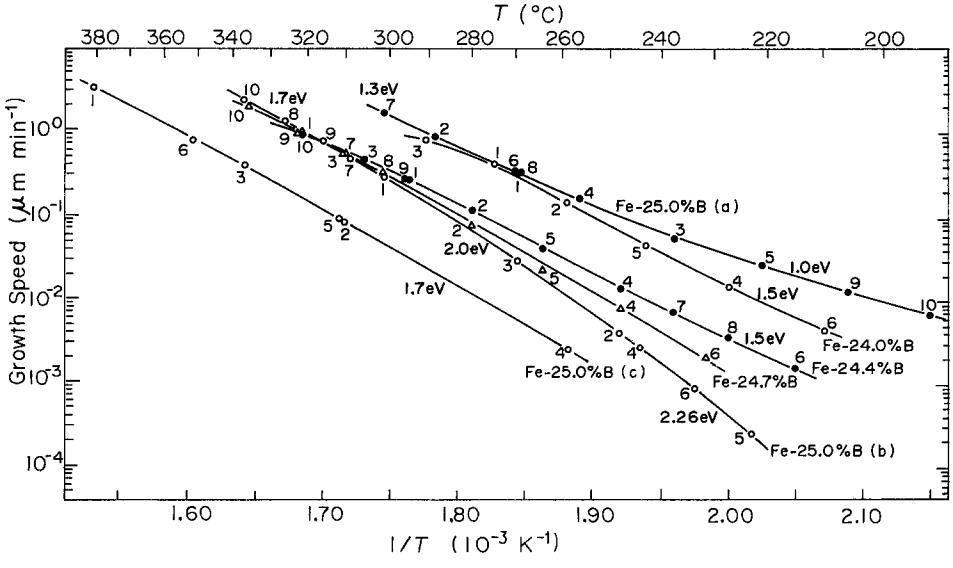

Figure 9 A summary of Arrhenius plots of the growth rates of various crystallites in various amorphous specimens. Numerals on each line represent the order of observations. (a), (b), and (c) represent the curves from different specimens with the same composition, Fe–25.0 at% B.

thermal growth curves were always straight, irrespective of small concentration deviations from the 3:1 stoichiometry, no temperature hysteresis of the growth speed appeared, as shown in Fig. 8 and 9, and no trace of change of boron concentration in α-iron particles and in the amorphous matrix was found. This means that the growth process of Fe_3B crystallites in 25 at% B amorphous alloy is not influenced by the long-range diffusion of boron but presumably by the reactions at the amorphous–crystalline interface. In this respect, the first objective of the present study seems to be fulfilled. On the other hand, unexpected complications in the crystallization behaviour, which would have already existed in the past experiments but probably have been masked by the effect of boron diffusion, appeared. The morphology of crystallization was complicated, exhibiting various types of precipitates, the growth rates of bct Fe_3B crystals were different from specimen to specimen almost independently of small deviations in boron concentration, and the Arrhenius plots of the growth rates did not always give straight lines but very slightly convex, concave, and sigmoidal curves, giving rise to the dispersed values of activation energy around 2.0 eV.

The above new findings in the crystallization behaviour of Fe–B amorphous alloys with exact or nearly 3:1-stoichiometric composition are analysed in the following section, taking account of local kinetic reactions at the amorphous–crystalline boundaries, and not of long range diffusion of boron.

4.2. Analysis of growth curves and models of reaction kinetics

The result of the present investigation tells us that the reactions of crystal growth process at the interface are not so simple as to be represented by a single rate equation even if the long range diffusion of boron is not included.

As a basis of the reaction kinetics, consider a crystal growth rate induced by a single rate process which may be represented by the equation,

$$v = a\beta\nu \exp(-E/kT) \qquad (1)$$

where a is the distance travelled by the boundary when one atom at the boundary is rearranged as a unit process from the disordered to the ordered site, β is a geometrical factor containing the ratio of the effective directions of motion and all possible directions in the atomic vibration, fraction of the number of available sites along the boundary, and the multiplicity factor of necessary motions for the rearrangement, ν is the frequency of atomic vibration, E is the activation energy of atomic rearrangement, k is the Boltzmann constant, and T is the absolute temperature. The reactions for the backward motion of the boundary can be neglected when the chemical potential difference between the amorphous and crystalline state is large enough, say ~ 1 eV. The vibrational entropy difference can be included in β, and the value of the latter is roughly estimated as $10^{-2\sim 3}$. a and ν are estimated to be of the order of 0.2 nm and $10^{13}\,\mathrm{sec}^{-1}$, respectively. Therefore, the theoretical consideration gives the value of the pre-exponential factor, $a\beta\nu$, as $\sim 10^{12}\,\mathrm{nm\,sec}^{-1}$. However, the actual values of the pre-exponential factor determined from the growth rate curves such as in Figs. 8 and 9 are $10^{15\sim 19}\,\mathrm{nm\,sec}^{-1}$. This large discrepancy between the measured and estimated values will be re-examined and discussed later. On the other hand, the value of the activation energy has been determined experimentally by the present and former investigations to be about 2.0 eV, but no theoretical calculation has been given for that.

When a relaxation in the growth rate appears, as in the previous experiment on 14 at% B alloy and other ones on the other nonstoichiometric composition alloys, Equation 1 must be modified as

$$v = a\beta\nu(-E/kT)R(t) \qquad (2)$$

where $R(t)$ is a function to take account of the changes in the interior and environment of the growing crystal during the time elapsed, t, mainly induced by the necessary long range diffusion of boron. Its simplest form will be

$$R(t) = \exp(-t/\tau) \qquad (3)$$

where τ is the temperature-dependent relaxation time and its activation energy was determined to be 4.8 eV in the previous experiment. It is unnecessary to employ the term, $R(t)$, in the present experiment, since no relaxation phenomenon existed, as mentioned before. Instead of that, the equation must be modified in a different way to take the temperature dependence of the apparent activation energy, or slight bending of the Arrhenius plot of the growth rate, and the above-mentioned extraordinarily large value of the pre-exponential term into consideration.

In general, when the temperature dependence of the activation energy appears, one could assume the underlying mechanism for that in two different ways; one is that the process is not single but composed of several distinct processes connected in parallel or in series, and the other is that the temperature-dependent structural change reversibly induces the activation energy change. The result obtained in the present investigation can be analysed in two ways, accordingly, as follows:

(a) Analysis by the assumption of composite process

When n different reactions take place in parallel at the boundary in the crystal growth process, the growth rate will be expressed by

$$v = \sum_n C_n a \nu_n \beta_n \exp(-E_n/kT) \qquad (4)$$

where C_n is the fraction of the nth reaction, which needs the activation energy, E_n, and satisfies the relation, $\Sigma_n C_n = 1$. The parameters ν_n and β_n are the vibrational frequency and the geometrical factor of the nth process, respectively. Which subprocess becomes predominant depends upon the value of the pre-exponential term and the temperature. The apparent activation energy of the overall process is found by the differential.

$$E = -k\frac{\partial(\ln v)}{\partial(1/T)} = \frac{\sum_n C_n A_n E_n \exp(-E_n/kT)}{\sum_n C_n A_n \exp(-E_n/kT)} \qquad (5)$$

where

$$A_n = a\beta_n\nu_n$$

Each frequency factor, $C_n a\beta_n\nu_n$, will be small, since C_n is smaller than 1. The temperature dependence of the activation energy is found by the further differentiation,

$$\frac{\partial E}{\partial(1/T)} = -\frac{\sum_{n\neq n'} C_n C_{n'} A_n A_{n'} \exp\left(-\frac{E_n + E_{n'}}{kT}\right)\left(\sum E_n^2 - \sum_{n\neq n'} E_n E_{n'}\right)}{k\left[\sum_n C_n A_n \exp(-E_n/kT)\right]^2} < 0 \qquad (6)$$

This equation shows that the apparent activation energy will increase at high temperatures and the Arrhenius plot of the growth rate will be upward concave, as the curve (a) in Fig. 9 shows. By the parallel connection, however, the upward convex curves are not reproduced and extrapolation of the calculated curve cannot give the large value of the frequency factor which appears at high temperatures.

When the composite process is connected in series, the subprocesses with higher activation energies will be controlling at low temperatures and, as the temperature is raised, the processes occupying the large fraction in the total number of necessary jumps will become more influential. Let us consider the nth process, which has the migration speed,

$$v_n = a\beta_n\nu_n \exp(-E_n/kT) \qquad (7)$$

and occupies a fraction, C_n, in the total length of the process. Since the time required to pass the distance C_nD is

$$t_n = C_nD/v_n = \frac{C_nD}{a\beta_n\nu_n}\exp\left(\frac{E_n}{kT}\right) \qquad (8)$$

the average velocity in the whole composite process will be

$$v = D\Big/\sum t_n = \frac{1}{\sum_n \frac{C_n}{a\beta_n\nu_n}\exp\left(\frac{E_n}{kT}\right)} \qquad (9)$$

Like Equation 5, the apparent activation energy of the overall process can be obtained as

$$E = \frac{\sum \frac{C_n}{A_n} E_n \exp(E_n/kT)}{\sum_n \frac{C_n}{A_n}\exp(E_n/kT)} \qquad (10)$$

the value of which will be close to that of the most influential subprocess and have a slight temperature dependence. Similar to Equation 6, the temperature dependence of the apparent activation energy is given by

$$\frac{\partial E}{\partial(1/T)} = \frac{\sum_{n \neq n'} C_n C_{n'} A_n A_{n'} \exp\left(\frac{E_n + E_{n'}}{kT}\right)\left(\sum E_n^2 - \sum_{n \neq n'} E_n E_{n'}\right)}{k\left[\sum C_n A_n \exp\left(\frac{E_n}{kT}\right)\right]^2} > 0 \quad (11)$$

This means that the apparent activation energy becomes smaller with increasing temperature and its Arrhenius plot will be upward convex. It is noteworthy that, at low temperatures where the subprocess with a high activation energy, E_i, and small fraction, C_i, is controlling the process, the pre-exponential factor, $a\beta_i\nu_i/C_i$, will also be dominant, giving rise to an extraordinarily large value of the observed pre-exponential term, as mentioned before, because of the small value of C_i. The upward convex curves like (b) and (c) in Fig. 9 can be reproduced by the series connection of the composite process accordingly.

The above discussion suggests that the temperature dependence of the Arrhenius plot and the apparent activation energy as shown in Fig. 9 will be readily reproduced by the combination of parallel and series connections of the subprocesses. As a model to account for the afore-mentioned variety of the growth rate curves, a composite process with three elements may be sufficient. There are two possible modes of connection; one is to connect a subprocess in series with two parallel ones and the other a subprocess in parallel with two others in series. Since the extraordinarily large pre-exponential factor of the growth rate curve with higher activation energy at higher temperatures, like curve (a) in Fig. 9, cannot be explained by the former, we employ the latter. Then, the growth rate of the process will be given by

$$v = \frac{1}{\frac{C_1}{a\beta_1\nu_1}\exp\left(\frac{E_1}{kT}\right) + \frac{C_2}{a\beta_2\nu_2}\exp\left(\frac{E_2}{kT}\right) + C_3 a\beta_3\nu_3 \exp\left(-\frac{E_3}{kT}\right)} \quad (12)$$

where subscript 1 and 2 represents the subprocesses connected in series and 3 the third one connected in parallel with the two. A general tendency exhibited by this model is readily understood by the schematic drawing of the growth rate curve in Fig. 10, in which the subprocesses 2, 1, and 3 are dominant in the high, medium, and low temperature range, respectively, and a sigmoidal growth rate curve, like those at 24.0 at % B and 24.4 at % B alloy in Fig. 9, is reproduced. The observed upward concave curve of 25.0 at % B (a) is supposed to correspond to the medium and low temperature region of the calculated curve of Fig. 10, where the subprocesses 1 and 3 are controlling, and actually the curve (a) can be reproduced by using the values, $C_1 \sim 10^{-3}$, $E_1 \sim 1.3$ eV, $C_3 \sim 1$, and $E_3 \sim 1.0$ eV. On the other hand, the convex curves, (b), (c), and of 24.7 at % B are regarded as the high and medium temperature region of the calculated one, and for curve (b), for instance, a good fit is obtained by using $C_1 \sim 10^{-12}$, $E_1 \sim 2.4$ eV, $C_2 \sim 10^{-5}$, and $E_2 \sim 1.8$ eV.

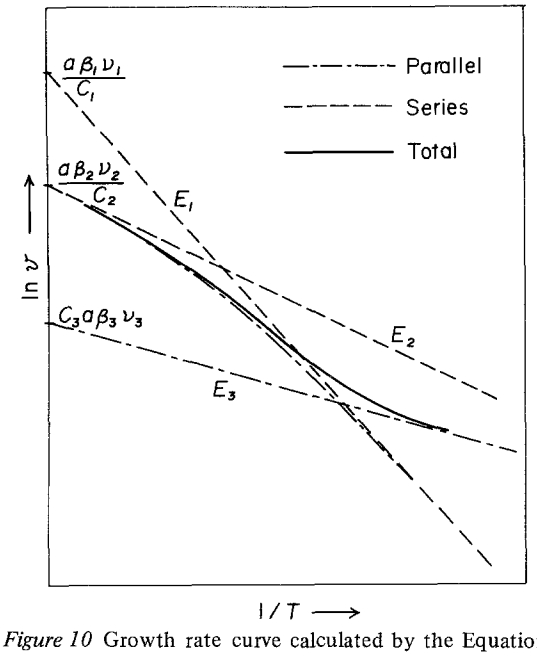

Figure 10 Growth rate curve calculated by the Equation 12 (full line) and those calculated for its component processes (dashed and dashed-and-dotted lines).

When a barrier process to slow down the boundary motion exists in the amorphous phase, it is considered in general to be connected in series with the process without barrier. For instance, when structural short- or medium-range order, such as chemical order clusters, already exists [24–26], resolution and reorientation of the ordered regions will be necessary before they are admitted into the crystalline phase, and thereby a subprocess with a high activation energy and a certain pre-exponential factor connected in series

with the ordinary atomic rearrangement process at the boundary must be considered. Another example of series connection is that, when a deviation from the 3:1-stoichiometric composition or concentration fluctuations exist in the amorphous matrix, diffusion of one constituent, most likely boron, will be required preceding the formation of the stoichiometric compound, Fe_3B, at the boundary, inevitably leading to the composite process model of series connection.

Parallel conncection is also conceivable in the Fe_3B crystallization process. Even when some barriers are formed at the phase boundary and the boundary motion is locally arrested, they could be passed and enveloped by the curved motion of the boundary. The model of series connection is no longer valid in such a case but at least partially has to contain the parallel connection. Another possible mechanism of parallel connection is that, to a site of crystal formation by atomic rearrangement on the phase boundary, there might be two mechanisms for atomic movement with different reaction parameters, one perpendicular to the boundary plane and the other along it, for instance, and these two are regarded as connected in parallel.

In Fig. 11 are schematically shown the structure in the vicinity of the growing crystalline–amorphous boundary and three kinds of subprocesses conceivable in the process of crystal growth. The process denoted by 1 is of the atomic rearrangement from the perfectly disordered region to the crystal, and that with subscript 3 is considered for the atomic movement along the boundary. In the centre of the figure is shown a small α-iron crystallite, which has been mentioned in the preceding paragraphs. Diffusion processes necessary for its formation must also participate in the whole growth process, and at least two mechanisms of that, i.e. volume diffusion and boundary diffusion as usually found in metals, must be taken into consideration. The necessary diffusion of one excess or deficit constituent, most probably of boron, will give rise to another composite character of the growth process when combined with the short-range atomic rearrangement at the boundary, as mentioned before. Nevertheless, if long-range diffusion appreciably and necessarily took place during the crystal growth, irreversible changes in the process would result when the temperature was alternately changed up and down, and difficulty in amending the discrepany with the experimental result would be encountered. But, it must be noted that, if the boron diffusion is allowed only along the boundary, there will be no conflict between the composite process model and the experimental fact that there is no temperature hysteresis.

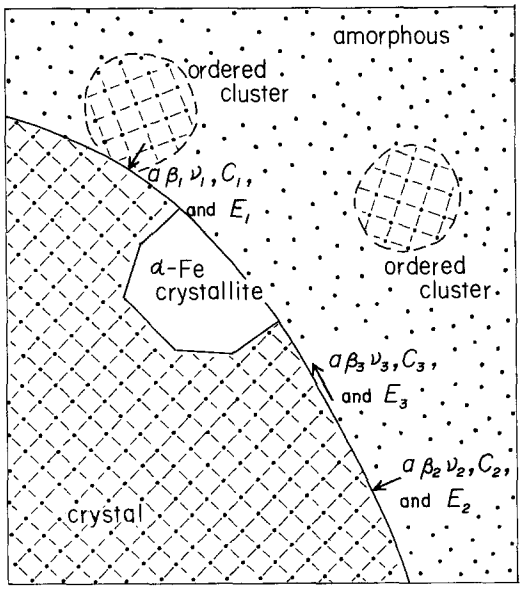

Figure 11 A sketch of the structure in the vicinity of the boundary of a growing Fe_3B crystallite. Three possible subprocesses of the growth are shown by arrows.

In the model calculation shown in Fig. 10, it is assumed that processes 1 and 2 are in series, process 3 is in parallel with that series, and $E_1 > E_2 > E_3$. These conditions will be satisfied when the three processes are assigned as described before. However, the assignments are only tentative and the final identification of the subprocesses and connection modes are still difficult because of a large variety in the possible mechanisms. Therefore, we will not further discuss the analysis of the growth rate curves based on the composite process models. But, instead, let us examine a fairly different way of analysis in the following paragraph.

(b) Analysis based on the assumption of reversible change of activation energy

Microscopically, the amorphous structure is not uniform but all constituent atoms are in different environments and static fluctuations of density and concentration may exist. Therefore, when the temperature is raised, uniform thermal expansion of the disordered lattice will not take place but non-uniform relative displacements of atoms will occur as a reversible structural relaxation. This

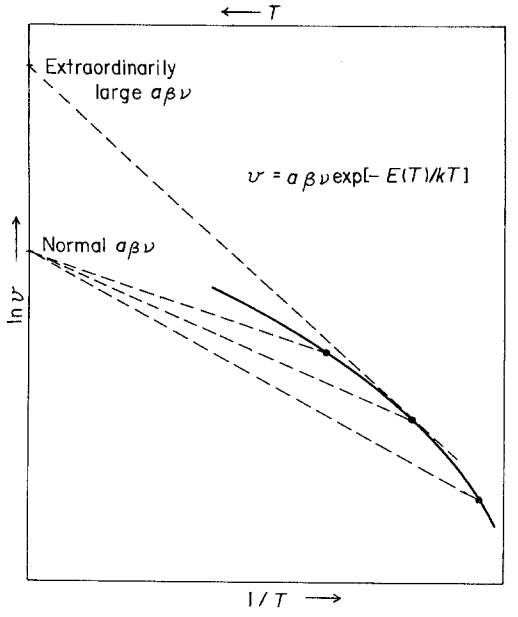

Figure 12 Schematic diagram to determine the temperature-dependent activation energy for a growth rate curve with the assumption of a single activation process with a constant pre-exponential factor.

reversible local change of structure will be especially remarkable in the relatively open region where the atomic jumps and rearrangements predominantly take place [27]. It is probably not unreasonable to consider such a reversible structural change at the boundary of the growing crystal and thereby a reversible change of activation energy for the crystal growth. This means that in the analysis of the growth rate curves, the assumption of a temperature-dependent activation energy could be employed and the observed anomalies in the growth rate curves could be accounted for.

First, we assume that the growth process simply follows Equation 1, where the value of E is a temperature-dependent variable, $E(T)$. Then, instead of the extraordinarily large pre-exponential factor $a\beta\nu$, which is obtained by extrapolating the tangent of the growth rate curve at any desired temperature as Fig. 12 shows, one can set up a reasonable value of the pre-exponential factor on the coordinate axis, from which a straight line can be drawn to any point on the growth rate curve and the temperature-dependent activation energy is determined from the inclination of the line, as the drawing in Fig. 12 shows. For example, when 10^{10} nm sec^{-1} is assumed for $a\beta\nu$ as mentioned before and the diagram like Fig. 12 is constructed, the activation energies of the specimens, Fe–25.0 at % B (a), (b), and (c) in Fig. 9 will exhibit the temperature dependence shown in Fig. 13. The values at various temperatures are not always in accord with those calculated from the tangents of the growth rate curves in Fig. 9 and entered in that figure. A general tendency read from the curves in Fig. 13 is that the activation energy becomes lower as the temperature increases. This is in good agreement with the presumption that non-uniform thermal expansion will take place especially in the less dense regions, where atomic jumps and rearrangements preferentially occur and the activation energy will become lower accordingly. A computer calculation on the diffusion process in an amorphous structure having density fluctuations of a certain extent actually showed a decrease of the activation energy with the increasing temperature [27].

Differences in the values of activation energy and probably of frequency factor and diversity in their temperature dependences between different specimens could be understood in the following way: density and concentration fluctuations, including the amount and degree of short range and medium range structural order, may be different from one to another among the specimens and

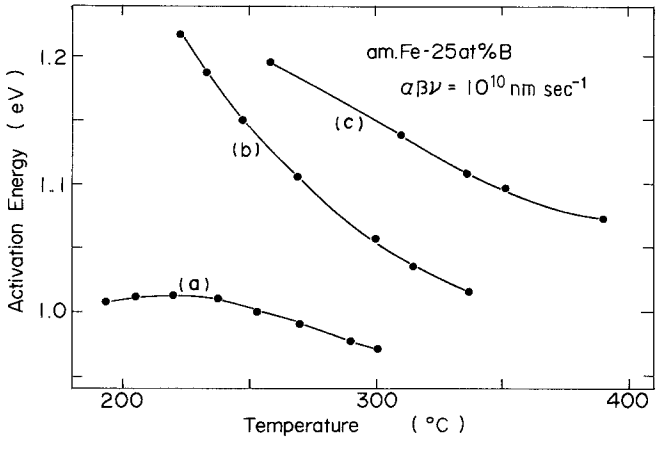

Figure 13 The temperature-dependent activation energies of the specimens, Fe–25.0 at % B (a), (b), and (c) determined by the diagrammatic analysis shown in Fig. 12, putting $a\beta\nu = 10^{10}$ nm sec^{-1}.

from place to place even in one specimen. These small differences could control the crystal growth process, giving rise to the differences in the values of the activation parameters. A similar consideration could also be taken when the composite-process model is employed.

The above two different interpretations based on the composite-process model and the temperature dependent activation energy model, respectively, seem to be equally effective and compatible in the analysis of the crystal growth process in the Fe–25 at% B amorphous alloy. Although no attempt to combine the two ideas or to select one of them has been made in the present study, this seems to require further investigation to find which gives the larger contribution and how to connect the two effects in the analysis of the process. A new experiment with very well controlled specimens such as of the 3:1 stoichiometric concentration and with known different degrees of order, which are extremely difficult to obtain though, could be the key to the solution of the above problem.

Acknowledgements

The authors wish to express their hearty thanks to Dr R. Oshima and other laboratory members for their valuable help in specimen preparation and electron microscopy. Thanks are also due to Mr I. Nonogaki for his continuous and useful discussions since his co-operation in the previous study.

References

1. K. F. KELTON and F. SPAEPEN, Proceedings of the 4th International Conference on Rapidly Quenched Metals (RQ-4), Sendai, August, 1981, edited by T. Masumoto and K. Suzuki, (Japanese Institute for Metals, Sendai, 1982) Vol. 1, p. 527.
2. B. FOGARASSY, Á, CZIRÁKI and I. SZABÓ, *ibid.* Jap. Inst. Metals Vol. I, p. 651.
3. J. W. DRIJVER, A. L. MULDER and S. RADELAAR, *ibid.* Vol. I, p. 535.
4. P. H. SHINGU, K. SHIMOMURA, R. OZAKI, K. OSAMURA and Y. MURAKAMI, Proceedings of the 3rd International Conference on Rapidly Quenched Metals, Brighton, August, 1977, Vol. I, edited by B. Cantor (The Metals Society, London, 1978) p. 315.
5. A. KURSUMOVIĆ, R. W. CAHN and M. G. SCOTT, *Scripta Metall.* **14** (1980) 1245.
6. L. LEONARDSSON and B. ANDERSON, Proceedings of the 4th International Conference on Rapidly Quenched Metals, Sendai, August, 1981, Vol. I, edited by T. Masumoto and K. Suzuki (Japanese Institute for Metals, Sendai, 1982) p. 579.
7. K. ZÁVETA, B. SPRINGMANN, J. Schneider, E. KROTOCHVILOVÁ, *ibid.* p. 523.
8. T. MASUMOTO, Y. WASEDA, H. KIMURA and A. INOUE, *Sci. Rep. Res. Inst. Tohoku Univ.* **A26** (1976) 21.
9. M. KIJEK, D. AKHTAR, B. CANTOR and R. W. CAHN, Proceedings of the 4th International Conference on Rapidly Quenched Metals, Sendai, August, 1981, Vol. I, edited by T. Masumoto and K. Suzuki (Japanese Institute for Metals, Sendai, 1982) p. 573.
10. A. L. GREER, C. J. LIN and F. SPAEPEN, *ibid.* p. 567.
11. F. E. LUBORSKY and F. BACON, *ibid.* p. 561.
12. R. OSHIMA and F. E. FUJITA, *Suppl. Sci. Rep. RITU* **A28** (1980) 8.
13. F. E. FUJITA, Atomic Energy Review, Suppl. 1 (IAEA, Vienna, 1981) p. 173.
14. U. GONSER, M. GHABARI, M. ACKERMANN, H. P. KLEIN, J. BAUER and H. G. WAGNER, Proceedings of the 4th International Conference on Rapidly Quenched Metals, Sendai, August, 1981, Vol. I, edited by T. Masumoto and K. Suzuki (Japanese Institute for Metals, Sendai, 1982) p. 639.
15. S. MORIMOTO, E. TORIKAI, A. ITO, K. SHIIKI and M. KUDO, *ibid.* p. 695.
16. H. MAEDA, H. TERAUCHI, N. KAMIJO, M. HIDA and K. OSAMURA, *ibid.* p. 397.
17. U. HEROLD and U. KÖSTER, Proceedings of the 3rd International Conference on Rapidly Quenched Metals, Brighton, August, 1977, Vol. I, edited by B. Cantor (The Metals Society, London, 1978) p. 281.
18. K. NUNOGAKI, Y. KATAO and M. KIRITANI, Proceedings of the 4th International Conference on Rapidly Quenched Metals, Sendai, August, 1981, Vol. I, edited by T. Masumoto and K. Suzuki (Japanese Institute for Metals, Sendai, 1982) p. 509.
19. Y. ISHIDA, H. ICHINOSE, H. SHIMADA and H. KOJIMA, *ibid.* p. 421.
20. T. HAMADA and F. E. FUJITA, paper submitted to *Jpn. J. Appl. Phys.*
21. H. P. SHINGU, M. CHUDO and R. OZAKI, *Suppl. Sci. Rep. RITU* **A28** (1980) 85.
22. M. W. RUCKMAN, R. A. LEVY, A. KESSLER and R. HASEGAWA, *J. Non-Cryst. Solids* **40** (1980) 393.
23. R. W. CAHN, J. E. EVETTS, J. PATTERSON, R. E. SOMEKH and C. K. JACKSON, *J. Mater. Sci.* **15** (1980) 702.
24. P. H. GASKELL, *J. Non-Cryst. Solids* **32** (1981) 165.
25. F. E. FUJITA, Proceedings of the 4th International Conference on Rapidly Quenched Metals, Sendai, August, 1981, Vol. I, edited by T. Masumoto and K. Suzuki (Japanese Institute for Metals, Sendai, 1982) p. 301.
26. T. HAMADA and F. E. FUJITA, *Jpn. J. Appl. Phys.* **21** (1982) 981.
27. M. KIRITANI and T. HAMADA, Proceedings of the 4th International Conference on Rapidly Quenched Metals, Sendai, August, 1981, Vol. I, edited by T. Masumoto and K. Suzuki (Japanese Institute for Metals, Sendai, 1982) p. 583.

Received 15 December 1983
and accepted 16 January 1984